IEEE Access
Multidisciplinary | Rapid Review | Open Access Journal

Received May 6, 2021, accepted May 17, 2021, date of publication May 28, 2021, date of current version June 21, 2021.

Digital Object Identifier 10.1109/ACCESS.2021.3084802

Design and Implementation of a Cost-Effective Wireless Charger for an Electric Bicycle

ALICIA TRIVIÑO-CABRERA, JOSE M. GONZÁLEZ-GONZÁLEZ, AND JOSÉ A. AGUADO, (Member, IEEE)
Escuela de Ingenierías Industriales, Universidad de Málaga, 29071 Malaga, Spain

Corresponding author: Alicia Triviño-Cabrera (atc@uma.es)

This work was supported in part by the Spanish Ministerio de Ciencia e Innovacion (MICINN) through the "Proyectos de I + D + i-RTI Tipo A" program under Project PID2019-110531-RA-I00, and in part by the II Plan Propio Smart-Campus by the University of Malaga.

ABSTRACT Wireless charging is a convenient method of charging Electric Vehicles (EVs). Its application has been widely studied for electric cars but so far there have been limited experiments for electric bicycles (e-bikes). This paper addresses the design process and implementation details related to a wireless charger for a specific e-bike. Some issues such as the position of the secondary coil or the control algorithm prove to be crucial to the performance of the wireless transfer. Concerning the placement of the secondary coil, the paper proposes and validates a theoretical model to quantify the effects of the surrounding interfering materials. A CC-CV (Constant Current - Constant Voltage) control algorithm has been implemented to validate the theoretical results in these two charging phases. The control, the coils and the compensation networks have been designed to be simple and robust. The theoretical model, the charger and its control have proven to be effective in a real 84-W e-bike.

INDEX TERMS Control, coil position, electric bicycle, wireless charger.

I. INTRODUCTION

Electric Vehicles (EV) constitute a sustainable mode of transport to cope with the greenhouse emissions generated by fuel-based vehicles. Of all electric vehicles, electric bicycles (e-bikes) are considered to be the most convenient form of transportation in the Smart City due to their low cost and maintenance, capability to operate in crowded environments and the fact that there is no need for licences or road taxes [1]. These advantages are helping to expand the e-bike market. In fact, it is expected to number up to 6.8 million units in 2024, which represents a 8.2% annual growth rate from 2016 [2]. The European region accounted for 20.12% of the global market, with the fastest growth occurring during the forecast period.

Wireless Power Transfer (WPT) can be foreseen as a suitable technology to promote the use of Electric Vehicles [3]. In the case of e-bikes in particular, WPT eases their charge process, makes the operation safer [4] and also broadens the scenarios in which the vehicle can be charged (even while moving) [5]. Although there are multiple technologies associated with WPT, the technology used most extensively for Electric Vehicles is inductive resonant WPT [3]. The basis of resonant WPT consists of two coupled coils referred to as the primary and the secondary coil. The primary coil is connected to the grid and, when powered, generates a time-varying magnetic field. The secondary coil must be placed so that it concatenates some of the generated magnetic field. This field will then induce a voltage on the secondary coil. As the secondary coil is connected to the EV battery, this component can be charged. More complex structures have been proposed with three [6]–[8] or four coils [9]. The power transfer is clearly affected by the relative position or misalignment between the primary and the secondary coils.

The use of inductive WPT in electric cars has already been tested in some prototypes and experiments, so we can conclude that they have reached a mature status [10]. However, so far a limited number of experiments have been conducted with other types of vehicles such as e-bikes. The application of this technology to e-bikes is not straightforward if we only consider the knowledge acquired in the context of electric cars. Firstly, weight and physical stability are critical in an e-bike. These two conditions can be compromised with the incorporation of bulky and heavy power components for the

The associate editor coordinating the review of this manuscript and approving it for publication was Mouloud Denai.

wireless charge. Secondly, the costs need to be much lower than for a car. The maintainability must also be minimized in order not to lose the advantages of this kind of transportation. With these requirements in mind, the design of these systems focuses on the particular features of an e-bike battery. Currently, the most popular types of batteries in e-bikes are the Li-Ion batteries [1]. These batteries are charged in a two-phase sequence. During the first phase, the battery is charged at a Constant Current (CC) until the battery reaches a voltage level. In the second phase, the battery is charged with the reached/Constant Voltage (CV) level until the current decreases to a predetermined threshold. The equivalent resistance of the battery during the process also varies. Moreover, the predefined current in the CC mode and the regulated voltage in the CV mode must be guaranteed even when the system suffers from a deviation from its standard operating conditions [11].

Thus, the key design steps of an e-bike wireless charger are the definition and position of the coils, the matching networks, the control strategy and the operational frequency. The main approaches to these subsystems are described next.

A core element in the wireless charger is the coupled coils. In electric cars, the secondary coil is placed underneath the chassis so that this element minimizes electromagnetic emissions inside the vehicle. The position of the secondary coil is more or less fixed and there has been no debate on this point. Indeed, there are new standards that fix the coil in the aforementioned position [10]. However, other vehicles do not have this metallic structure and therefore the position of the secondary coil may be arbitrary. This is the case with e-bikes. The authors in [12] presents the design of two complex pairs of coils to be placed in the kickstand for a single or double support. The coils rely on ferromagnetic materials to improve the power transfer, which makes the charger more expensive than when using simple coils. Interference with other materials of the e-bike has not been considered, as the prototype does not include this type of vehicle. A series-resonant inductive system is proposed in [13] for a wireless charger. It also suffers from the same inconvenience as the previous approach because it includes an E-shape coil with ferromagnetic material. Alternatively, a bulky coil is placed in the base of the rear wheel in [5]. The volume and position of the secondary coil may restrict its applicability. The work in [14] proposes the placement of the secondary coil in a salient pole of the charging structure. The pole is inserted in the bicycle armature to increase the efficiency of the WPT while avoiding coil misalignment. Although the coupling coefficient is increased, this solution demands a structure for the charging station, which may also be prone to damage. A three-layer coil for the primary side and some switched capacitors are proposed in [15] to change from the CC to the CV mode. The work in [8] implements the power transmitter as two coils. One of the coils is only connected for the CV mode. As can be observed, these experiments rely on complex structures for the coils and have not addressed the most convenient position for these components.

Wireless chargers count on matching networks to make the system operate at resonance. The most simple topology is the Series-Series, as used in [13], but there are other multi-resonant approaches. The work in [16] proposes the use of switched capacitors and coils on the secondary side to have a different circuit when the battery is charged in CC or CV mode. In [4], the authors propose a S-LCC topology for the control of the CC-CV charging. On the primary side, there is a switch that activates/deactivates one capacitor for each mode. On the secondary side, a reactive network with two capacitors is implemented. As concluded in [17], [18], the Series-Series is the most cost-effective solution. The authors in [6] opt for two different capacitors in a Series-Series topology. One of the capacitors on the primary side is used for the CC mode and another for the CV mode.

Control algorithms are necessary to ensure a correct wireless power transfer under misalignment or different battery status. The work in [11] presents a control algorithm, which is tested in a real e-bike. The designed control sets the voltage output at 48 V so it does not implement the CC mode. The experiments, which were conducted for a linear load instead of a battery, show a low efficiency. The authors have not carried out an analysis of the best position for the secondary coil. In fact, the efficiency of their charge is very low (25-80 % for a coil gap of 0-10 cm), which could be derived from a magnetic leakage on the components of the bicycle due to the position selected for the secondary coil. Alternatively, the work in [17] varies the current according to the relative position of the coils. To extend the durability of the battery, it is preferable to perform the charge in a CC-CV mode. In addition, the work in [17] concludes that a cost-effective control algorithm should be preferred for e-bikes. The work in [6] uses some switches and two coils on the primary side to change the circuit process for a CC and a CV mode. In order to identify when to set the corresponding operation mode, the equivalent resistance of the battery is estimated. A perfectly-tuned Series-Series compensation network is assumed for this estimation.

As we have previously stated, it is important to reduce the costs and weight of the secondary side to make a commercial-grade e-bike charger appealing. Thus, the secondary structure should be reduced. This implies minimizing the additional components (coils and matching networks) and implementing a simple control algorithm for the CC and CV charging modes. Taking into account these requirements, we design, implement and test a wireless charger for a specific e-bike. The contributions of this work are twofold:

- Providing the details required for effective implementation of a wireless charger for an e-bike. In contrast to some previous works [4], [6], [7], [12], [13], [16], [17], the design has taken into account the impact of mounting the secondary coil on the vehicle. With this goal in mind, we propose a theoretical model, which includes the effects of the surrounding interfering materials. For some measurements, the model has been validated and tested on an e-bike instead of in a

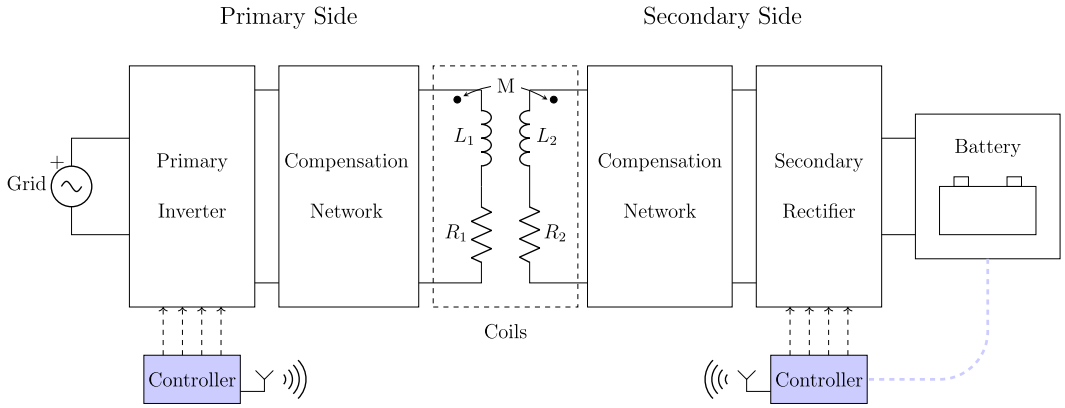

FIGURE 1. Generic diagram for magnetic resonance wireless chargers with compensation networks.

laboratory setting. As demonstrated theoretically and experimentally, the position of the secondary coil clearly affects the electromagnetic emissions and, in turn, the losses [19]. In contrast to [18], this work has evaluated the most convenient position of the secondary coil while keeping in mind its usability. The experimental results have revealed the impact of the position of the secondary coil on the system efficiency, temperature risks and electromagnetic emissions.

- Designing a low-cost and reliable secondary-side charger with a simple but effective control that manages the CC and the CV charging modes to illustrate the performance of the WPT system and compare it with the theoretical results derived from the proposed model. The defined control strategy does not rely on additional reactive components. A simple Series-Series compensation topology is used as in [8], but the CC and the CV charging modes are implemented as recommended for the Li-Ion batteries [1]. With this approach, the costs of the charger in the bicycle are reduced while its reliability is improved.

The remainder of the paper is structured as follows. Section 2 describes the equivalent circuit of the charger and presents the theoretical model used to quantify the losses caused by the surrounding interfering materials. This description is necessary for the design, as shown in Section 3, which addresses the implementation issues of this charger. In particular, it focuses on the three potential positions of the secondary coil and validates the theoretical model developed previously. Section 4 describes some related work on control algorithms for e-bikes and presents a simple but effective control algorithm, which will be used to validate the model. Section 5 presents the experimental characterization of the wireless charger when installed on the e-bike for the three positions analyzed. Finally, Section 6 summarizes the main conclusions of this paper.

II. THEORETICAL ANALYSIS

For our design proposal, we aim to use a simple but controllable wireless charger. We opted for one of the most simple structures of an EV wireless charger, as depicted in Figure 1. It does not include any DC/DC converter on the secondary side, which eases its implementation and control [11], [18].

This diagram is usually modelled as an electric circuit as shown in Figure 2. In this circuit, we have two coupled coils (L_1 and L_2) and their parasitic resistances (R_1 and R_2). M corresponds to the mutual inductance between the transmitter and the receiver. The matching networks follow a simple but effective Series-Series topology as in [13]. They are composed of capacitors C_1 and C_2. Although there are complex matching networks [16], the Series-Series compensation network has shown its effectiveness in coping with coil misalignment at a low cost [11].

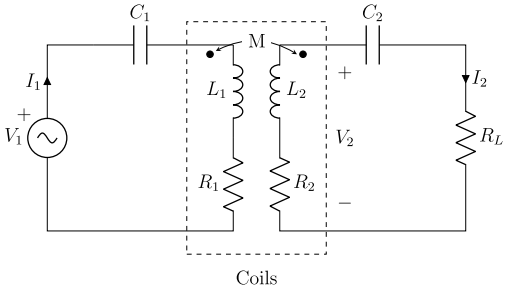

FIGURE 2. Core structure of a wireless charger with Series-Series compensation network.

In this simplification, the output inverter V_1 is a sinusoidal wave assuming a first harmonic approximation. The impedance of the battery at the input of the secondary rectifier is modelled as the resistance R_L (referred to as the equivalent load resistance). The relationship between the internal resistance of the battery R_{Bat} and R_L is expressed as follows:

$$R_L = \frac{8R_{Bat}}{\pi^2} \tag{1}$$

With a mesh-based analysis, we can state that:

$$\vec{V}_1 = \left(R_1 + j\omega L_1 + \frac{1}{j\omega C_1}\right)\vec{I}_1 - j\omega M\vec{I}_2 \tag{2}$$

$$\vec{V}_2 = \left[(R_2 + j\omega L_2)\,\vec{I}_2 - j\omega M\vec{I}_1\right] = \left(R_L + \frac{1}{j\omega C_2}\right)\vec{I}_2 \tag{3}$$

From the two previous equations, we can infer the input impedance Z_{in} as follows:

$$Z_{in} = \frac{\vec{V}_1}{\vec{I}_1} = R_1 + j\left(\omega L_1 - \frac{1}{\omega C_1}\right) + \frac{\omega^2 M^2}{Z_{22}} \tag{4}$$

where $Z_{22} = (R_2 + R_L) + j\left(\omega L_2 - \frac{1}{\omega C_2}\right)$

In order to have a purely ohmic input impedance, the reactive term must be null. This condition is expressed with the following equation:

$$\omega L_1 - \frac{1}{\omega C_1} = -Imag\left(\frac{\omega^2 M^2}{(R_2 + R_L) + j\left(\omega L_2 - \frac{1}{\omega C_2}\right)}\right) \tag{5}$$

After developing this further, we obtain:

$$\omega L_1 - \frac{1}{\omega C_1} = \frac{\omega^2 M^2 \left(\omega L_2 - \frac{1}{\omega C_2}\right)}{(R_2 + R_L)^2 + j\left(\omega L_2 - \frac{1}{\omega C_2}\right)^2} \tag{6}$$

This last equation is verified when the two pairs of coils and their corresponding capacitor constitute two independent resonant tanks at the same operational frequency (ω_0).

$$\omega_0 = \frac{1}{\sqrt{L_1 C_1}} = \frac{1}{\sqrt{L_2 C_2}} \tag{7}$$

Thus, to design an SS compensation network, the capacitors can be defined with their corresponding coils once the frequency is set according to the application specifications.

The system efficiency is defined as the ratio between the active power delivered to the load and the active power generated by the source. This parameter can be formally expressed as:

$$\eta = \frac{R_L I_2^2}{R_1 I_1^2 + R_2 I_2^2 + R_L I_2^2} = \frac{R_L}{\frac{R_1 I_1^2}{I_2^2} + R_2 + R_L} \tag{8}$$

From Equation (3), we can infer the relationship between the modules of the I_1 and I_2 currents.

$$\left|\frac{I_1}{I_2}\right| = \frac{R_2 + R_L}{\omega_0 M} \tag{9}$$

So that the system efficiency is equal to:

$$\eta = \frac{R_L}{R_1\left(\frac{R_2 + R_L}{\omega_0 M}\right)^2 + R_2 + R_L} \tag{10}$$

In order to maximize the efficiency, the denominator of the previous expression should be minimized. This implies that:

$$\frac{R_2 + R_L}{\omega_0 M} \ll 1 \tag{11}$$

Thus,

$$\omega_0 \gg \frac{R_2 + R_L}{M} \tag{12}$$

If the relationship in Equation (12) holds, the efficiency corresponds to:

$$\eta \cong \frac{R_L}{R_2 + R_L} \tag{13}$$

As a conclusion, we can state that a perfectly-tuned Series-Series system keeps its efficiency in a wide range of gaps. For an efficient power transfer, it is desirable to minimize the ratio R_2/R_L.

However, the coils will not be isolated in a real prototype. In fact, there will be other conductive materials of the vehicle surrounding the coils, which will alter the equivalent circuit. In this paper, we model their effects in the circuit analysis by incorporating only one additional mesh. This model represents an application of the approach derived in [20], where two additional meshes were incorporated to model the two types of shielding materials. In our model, we mainly have one single interfering material so we modified the previous model to adapt to this condition. This new mesh is composed of a resistance (R_3) and an inductor (L_3), with the latter element coupled with the primary and the secondary coils. This effect is illustrated in Figure 3.

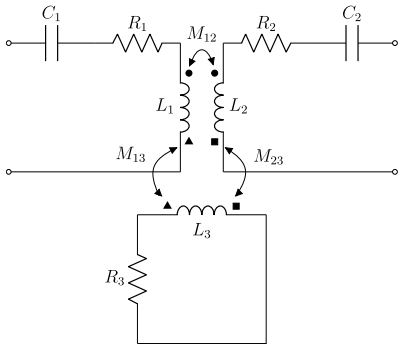

FIGURE 3. Model of the core structure of the e-bike and the surrounding interfering materials.

R_3 and L_3 model the losses caused by the interfering materials. In particular, R_3 models the conductive losses. As presented in [20], the resistance of a plate can be approximated to:

$$R_3 \propto \sqrt{\rho f \mu} \tag{14}$$

where ρ and μ are the resistivity and the permeability of the interfering material respectively.

With circuital simplifications, it is possible to derive the equivalent coupler in Figure 4.

The values of these components in the simplified model are:

$$Z'_{11} = Z_{11} + \frac{\omega^2 M_{13}^2}{Z_{33}} \tag{15}$$

$$Z'_{22} = Z_{22} + \frac{\omega^2 M_{23}^2}{Z_{33}} \tag{16}$$

$$M'_{12} = M_{12}\left(1 - \frac{K_{13} K_{32}}{K_{12}}\right) \tag{17}$$

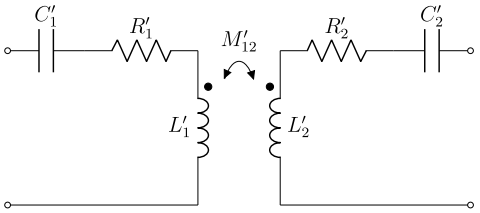

FIGURE 4. Simplified equivalent circuit of a coupler with surrounding (ferromagnetic and metallic) materials.

where $Z_{33} = j\omega L_3 + R_3$, $Z_{11} = j\omega L_1 + \frac{1}{j\omega C_1} + R_1$, $Z_{22} = j\omega L_2 + \frac{1}{j\omega C_2} + R_2 + R_L$ and K_{12}, K_{13} and K_{32} are the coupling coefficients associated to M_{12}, M_{13} and M_{32} respectively.

If we further analyse this last expression, we can derive that:

$$Real\left(Z'_{11}\right) = R'_1 = R_1 + \frac{\omega^2 M_{13}^2}{|Z_{33}|^2} * R_3 \tag{18}$$

$$L'_1 = L_1 - \frac{\omega^2 M_{13}^2}{|Z_{33}|^2} * L_3 \tag{19}$$

$$Real(Z'_{22}) = R'_2 = R_2 + \frac{\omega^2 M_{32}^2}{|Z_{33}|^2} * R_3 \tag{20}$$

$$L'_2 = L_2 - \frac{\omega^2 M_{32}^2}{|Z_{33}|^2} * L_3 \tag{21}$$

Thus, the self-inductances and the new mutual inductance of the equivalent coupler are lower than in the configuration of the original coils without the conductive materials [21]. As for the resistances, they are increased. In the particular case of the e-bike, the effects are expected to be more severe on the secondary side due to its proximity to the interfering material, so the parameters of the equivalent secondary side will change more noticeably. With regard to Equation (10), the efficiency will also be reduced as the new R_2 will be higher. The system in a real bicycle will also experience a lower output power as the equivalent mutual inductance decreases. Since the value of R'_2 is dependent on R_3 as expressed in Equation (20), the greater the resistance of the interfering materials and their size, the greater the increase of R_2. Thus, R'_2 is dependent on the interfering materials, i.e. on the position of the secondary coil. The efficiency and the power transfer are both affected by the placement of this component in a real e-bike. This effect is not reflected in the experiments conducted without a real vehicle.

When connected to the battery, we can work with the input impedance of the wireless charging coupler. In a real vehicle, the input impedance is equal to:

$$Z'_{in} = \frac{\vec{V}_1}{\vec{I}_1} = Z'_{11} - \frac{\omega^2 M'^2_{12}}{Z'_{22}} \tag{22}$$

Different positions of the secondary coil are associated with a different distribution of the surrounding materials. Thus, they will experiment different input impedances.

So far, we have described the efficiency related to the coupler, but a real prototype will also be affected by the efficiency of the power converters, as we will explain in Section 5.

III. COIL DESIGN AND PLACEMENT

Similarly to the approach proposed in [3], we first list the requirements imposed on the WPT charger for an e-bike. The identified requirements are:

- Low cost
- Low weight
- Avoiding the heating of some metallic structures of the bicycles due to the magnetic field. This could affect the safety of the charge and affect the users' health.

One of the key phases in the design of the wireless charger is the coil design. In this particular case, misalignment may not be so severe, as the bicycle can be supported by an auxiliary platform that can guarantee the position of the vehicle during the charge process (e.g. Daymak drive system). Due to their simplicity, the topologies analysed for the e-bike coils were the square and circular ones without additional ferromagnetic materials, to obtain low-cost components. Alternative options such as DD or DDQ were discarded as they result in more expensive coils [3].

For the e-bike in question (Torrot City Surfer), we designed two circular coils with the following features:
where $r_{1,in}$ and $r_{2,in}$ are the internal radius of the primary and the secondary coil respectively. The variables $r_{1,out}$ and $r_{2,out}$ are the external radius of the primary and the secondary coil and N_1 and N_2 are the number of turns of both coils. For a separation of 7 cm, the mutual inductance is $13.1\mu H$. These dimensions have been carefully selected to represent: (i) a negligible additional weight in comparison with the e-bike (21 kg) and (ii) an element that could be easily inserted in the bicycle wheel. The next image shows the implementation of the coils. The coils are built with Litz-wire in order to reduce the skin effect at the operating frequency.

The operating frequency is selected as 85 kHz. In this way, the charger can comply with international recommendations for EV chargers, in case e-bikes are included in the future [10]. As mentioned in Section II, the prototype has been designed following a Series-Series topology as it allows for simple control. This topology uses one capacitor in series with the coil on each side of the charger. Their capacitance value depends on the self-inductance of the coils and is computed using (7). For the coils defined in Table 1, the capacitance values for the matching network are:

TABLE 1. Parameters of the developed coils.

Primary coil		Secondary coil	
L_1	150.47 μH	L_2	27.08 μH
R_1	195.01 mΩ	R_2	22.89 mΩ
r_1, in	5 cm	r_2, in	1.5 cm
r_1, out	11 cm	r_2, out	7 cm
N_1	28	N_2	20
M	13.04 μH		

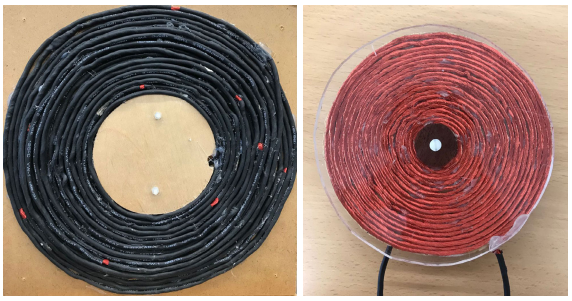

(a) Primary coil (b) Secondary coil

FIGURE 5. Implementation of the coils.

TABLE 2. Parameters of the matching network.

Capacitor	Theoretical value [nF]	Measured value [nF]
C_1	24.43	24.85
C_2	135.83	145.52

The matching network has been made using polypropylene capacitors because their good performance under high frequencies makes them suitable for this prototype.

One of the goals of the paper is to evaluate the ideal position of the coils in a real bicycle, which could differ from what is expected. In fact, the positioning of the coils constitutes one of the main difficulties with this kind of EV wireless charger. In electric cars, the position of the secondary coil is not a concern as it is always installed under the chassis of the vehicle. In contrast, there is no fixed position for the secondary coil on e-bikes. Moreover, its placement will impact on the bike's stability, the charger efficiency and even the feasibility of using the bike immediately after the charging process because of derived heat problems. As presented in the previous section, the surrounding materials alter the equivalent resistance of the developed model and, in turn, other performance metrics are also altered. In order to validate the previous model, we have set three tentative positions for the coil on the e-bike taking into account the quantity of interfering materials found nearby. In particular, we have studied the materials used in the Torrot City Surfer e-bike. There are two representative placements on the front wheel, and one close to the seat. The proportion of the surrounding materials is similar on the back wheel, and so the effects are assumed to be alike to those obtained in two of the positions tested. The alternative position on the bicycle frame was ruled out, as initial tests showed that the battery suffered from a noticeable increase in temperature, which may cause some damage. Other complex placements, which were not feasible in a pre-built bicycle, were also omitted. Thus, the positions analysed are:

For the tentative positions, we have derived the percentage of interfering material in a circular area with a diameter equal to twice the radius of the secondary coil. Through an image analysis, we have quantified the number of pixels associated to the interfering materials, i.e. air, aluminum and plastic.

(a) Position A (b) Position B (c) Position C

FIGURE 6. Coil positions analysed.

TABLE 3. Percentage of surrounding materials for the positions analysed.

Pos.	Air [%] μ:$1.25 \cdot 10^{-6}$ ρ: $1.3 \cdot 10^{16}$	Plastic [%] μ:- ρ: $10 \cdot 10^{20}$	Aluminium [%] μ:$1.25 \cdot 10^{-6}$ ρ: $3.9 \cdot 10^{-8}$
A	46	23	31
B	43	25	32
C	40	60	0

Units: $\mu[H/m]$, $\rho[\Omega m]$

TABLE 4. Modelled input impedance.

Position	Module [Ω]	Angle [rad]
Not mounted	2.69	0.45
A	4.218	0.47
B	4.24	0.18
C	3.59	0.19

Please note that the magnetic properties of these materials are quite different. The results are summarized in Table 3.

According to Equation (21), the input impedance of the positions is affected by the way in which the interfering materials modify the parameters of the equivalent circuit in Figure 4. We have conducted multiple tests to validate this model. In particular, for the three tested positions we have measured the relationship between the input voltage and the input current. From these measurements, we have derived a linear relationship. The proportional constant is a complex number, which represents the input impedance. The next Figure reflects the module of the input impedance for the three positions tested and for the situation in which the coils are not mounted on a vehicle.

The variation of the input impedance is a consequence of modifying the parameters in the model presented in Figure 3. Table 5 reflects this effect for the three positions tested in a real e-bike. In particular, the Torrot City Surfer has been used for these experiments, along with an LCR meter. There are notable changes in the measured resistance of the secondary coil for each of the three positions. As predicted by the model, the resistance levels of the coils increase when they are surrounded by interfering materials (Equations (18) and (20)), whereas the inductances decrease (Equations(17), (19) and (21)).

An alternative to this model is Finite Element Analysis (FEA) software. However, this software tool requires some expertise on how to proceed with the surface triangle mesh, which may not be easily acquired. In addition, FEA

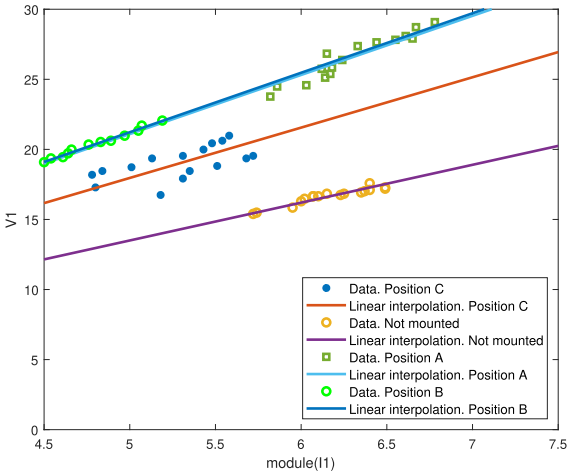

FIGURE 7. Linear interpolation of the measurements as an input impedance.

TABLE 5. LCR measurements.

	L1[μH]	**R1**[$m\Omega$]	**L2**[μH]	**R2**[$m\Omega$]	**M**[μH]
Not mounted	150.47	195.01	27.07	22.89	13.04
A	147.72	452.70	26.74	58.20	11.45
B	148.76	189.50	26.93	492.01	12.02
C	150.33	206.50	26.86	22.71	12.82

simulations are computer-based and time-consuming, which may delay the design process considerably.

IV. PROPOSED ROBUST AND SIMPLE CONTROL

To extend the durability of lithium-ion batteries, they must be charged with a two-phase method referred to as CC/CV [3]. This strategy consists in charging the battery at constant current until the maximum battery voltage recommended by the battery manufacturer is reached. When this happens, the charge is regulated so that the voltage is kept constant. The value of the charging current is also chosen based on the characteristics of the battery, although values lower than the recommended maximum help to extend the battery lifespan.

One of the goals of this paper is to evaluate the developed model to determine the effects of the interfering materials on a complete CC-CV charge. The following figure shows an example of a theoretical CC/CV charging application for the battery used in the prototype. It has a first constant-current stage at 2 A in which the voltage increases, followed by a constant-voltage stage at 42 V in which the charging current gradually decreases. During the charge process, the equivalent resistance of the battery changes with an increasing non-linear function.

This control technique has been applied in the literature for generic EV wireless chargers using several strategies. The variants mainly depend on the converter in which they operate and the communication systems used. In addition, the proposal in [22] modifies the topology to include switches to commute the devices operating in each phase. Apart from the bulky switches, this proposal presents a main limitation

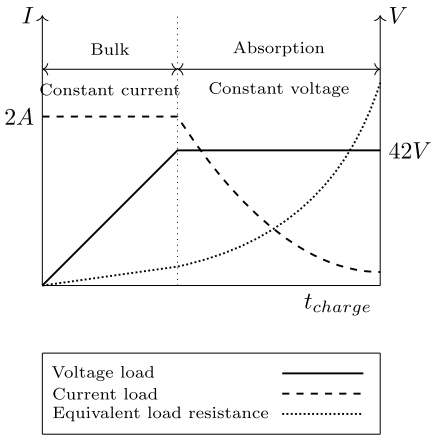

FIGURE 8. CC/CV charge.

as it is not able to regulate the charging current or voltage. This shortcoming restricts the compatibility between different devices. In the field of power electronics design, it also presents other drawbacks, such as greater design complexity and an increased number of components. It results in a higher cost and weight in a system that seeks to reduce both of these to a minimum. The authors in [23] also apply a strategy in which the charger topology is modified. Specifically, they opt for a dual full-bridge inverter and a PI control, which makes the system more complex.

Conversely to what is observed when switches are added, options based solely on adjusting the operation of the converters result in simpler systems, which are more convenient for an e-bike charger [24]. Relying on communications between primary and secondary sides allows for the application of simpler and equally robust control strategies, as shown in [23]. The authors use a dual parallel PI controller installed on the primary side. There are two PI controllers: one for the current regulation and another for the voltage regulation. A selector forces only one controller to be active depending on the charging mode. Cascade PID controller solutions improve the transition between both charging modes. This solution is applied in [25], but the controller adjusts the grid controlled rectifier instead of the primary inverter. As a consequence, it is necessary to incorporate a Phase Locked Loop (PLL).

Our proposal opts for a simplified approach, as shown in [26] but with two main simplifications. Firstly, there is no need to use intermediate coils, which means that the design process and its implementation are easier in comparison with [26]. Secondly, we include an automation for the selector, which avoids the manual switching for the two charging phases. These modifications ensure the proper application of the two-phase charging while minimizing the required computational resources. This simplification could report in a reduction of the controller. The control scheme is depicted in Fig. 9. As can be observed, only one PI controller is included.

The control works as follows. Firstly, the current and the voltage (I_m and V_m) are acquired from the battery connection

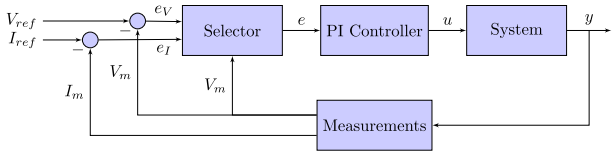

FIGURE 9. Control scheme for CC/CV charging.

and sent to the primary side via a wireless communication channel. On the primary side, the measurements are received and processed. The primary control includes two comparison blocks, a selector and a PI controller. During the first charging phase, the charger must operate in the CC mode. The selector has been automated so that the controller receives the current error ($I_{ref} - I_m$) as long as the voltage is lower than V_{ref}. V_{ref} corresponds to the maximum indicated by the battery manufacturer. When reached, it means that the CV phase should start. If this occurs, the controller receives the voltage error. It is important to highlight the fact that compatibility with other bikes is ensured as the charging references and the selector's decision are based on the battery parameters sent by the secondary controller. For our particular e-bike, V_{ref} and I_{ref} are 42 V and 2 A respectively, as shown in Figure 8.

Once the selector has chosen the proper error that must be considered, it transfers this data to the PI controller. The PI controller then adjusts the phase switching to apply to the primary inverter. Phase-shifting modifies the output voltage of the primary inverter, thereby regulating the battery charge.

Both the control and the wireless communications have been implemented in a Raspberry Pi, a small single-board computer with Bluetooth and IEEE 802.11 as wireless technologies. More specifically, a Raspberry Pi 4 has been used for the primary controller, while the Raspberry Pi Zero W has been used for the secondary controller. The choice of a different controller for the secondary side is due to the fact that, despite its lower processing capacity, it has very reduced energy consumption and size. As presented in the requirement lists, these two features must prevail in the e-bike wireless charger.

To comply with the CC/CV charging strategy of the proposed control, the secondary current and voltage measurements are required. The measurements are taken by the Raspberry Pi Zero W, which uses the I2C protocol to communicate with an Analog to Digital Converter (ADC) that converts the analog voltage and current measurements to digital form. These data are sent to the primary controller using a Bluetooth communication.

V. EXPERIMENTAL EVALUATION

An important goal of our work was to evaluate the performance of the potential configurations of the wireless charger and the control design in a real e-bike. The wireless charger was designed and implemented for an e-bike manufactured by Torrot, in the City Surfer model. In addition to the coils, the compensation networks and the controllers, we also included the power electronics necessary to generate the 85-kHz magnetic field as recommended by SAE J2954. The schematic is illustrated in Figure 10.

One of the biggest challenges for power electronics is the high switching frequency, which can lead to excessively high losses and temperature problems in converters. SiC MOSFETs are suitable switches for these converters, since their low drain-to-source ON-resistance makes it possible to reach high frequencies while maintaining reduced dissipation needs. Specifically, the full-bridge inverter has been implemented using two evaluation boards model KIT8020-CRD-8FF1217P-1 from CREE. This board includes two SiC MOSFET to constitute each of the inverter's legs. Figure 11 is an image of the primary side equipment. The full-bridge topology has been selected over the half-bridge even though it requires two additional MOSFETs. This is done for reliability purposes, as the current flowing through the converter is halved, which will lead to reduced losses and cooling needs in the conversion stage. This current also affects the losses in the coils. The secondary side includes a full-bridge rectifier composed of SiC diodes.

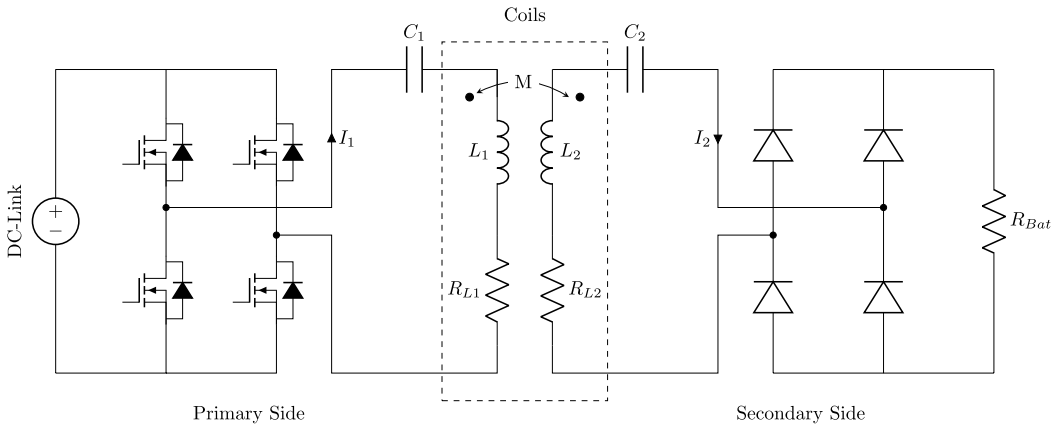

FIGURE 10. Scheme of the proposed charger topology.

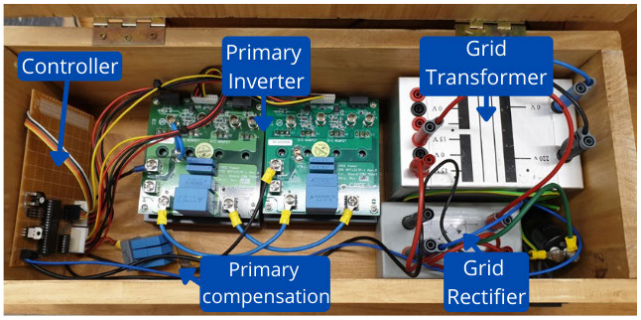

FIGURE 11. Picture of the primary side charger.

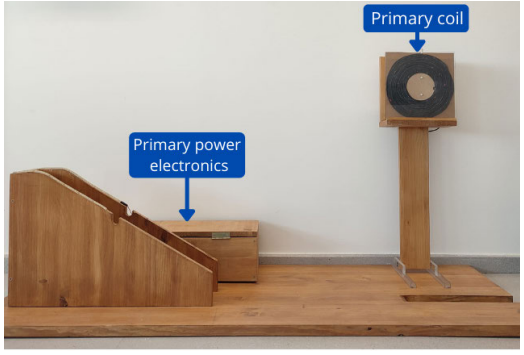

FIGURE 12. Picture of the pole with the primary coil.

Figure 12 shows the designed pole for the primary coil, which also has some wooden rails to reduce the misalignment effects. The three positions evaluated for the secondary coil are illustrated in Figure 13 for the secondary coil.

For these three positions, we have measured the rectifier input power and the inverter output power. From these two measurements, we have computed the efficiency of the charger as summarized in Table 6. The inverter and the rectifier currents and the rectifier input voltage are rms values. The experimental efficiencies are measured between the rectifier input and the inverter output, as performed in the theoretical analysis in Section 2. No control has been applied in these tests. For illustrative purposes, we have included two scopes of the rectifier input and the inverter output for position C in Figures 14 and 15 respectively.

TABLE 6. Performance evaluation for the tested positions of the secondary coil.

Parameter	Not mounted	Pos. A	Pos. B	Pos. C
Inverter output voltage	18.6 V	22.3 V	20.4 V	20.5 V
Inverter output current	6.5 A	6.78 A	6.7 A	6.36 A
Inverter power factor	0.978	0.894	0.987	0.893
Rectifier input voltage	44.5 V	44.5 V	44.8 V	43.9 V
Rectifier input current	2.48 A	2.58 A	2.51 A	2.22 A
Rectifier power factor	0.998	0.998	0.998	0.998
Experimental efficiency	93.17 %	84.79 %	83.17%	92.6 %
Modelled efficiency	93.28 %	82.02 %	81.51 %	92.7 %

(a) Position A. (b) Position B.

(c) Position C.

FIGURE 13. Tested positions of the secondary coils.

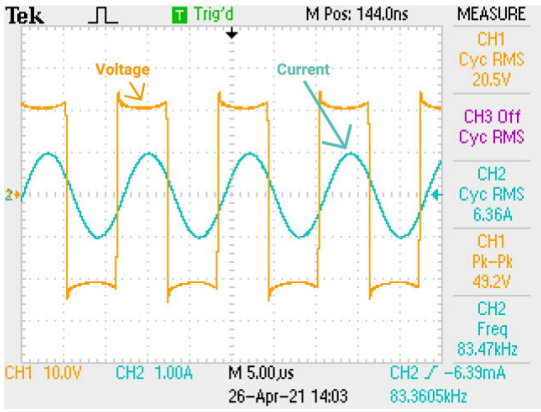

FIGURE 14. Voltage and current at primary inverter output (Position C).

As explained in Section 2, efficiency is affected by the modified resistances of the secondary and primary coils once the surrounding elements are taken into account. Based on Equation (10), the efficiency is computed with these new parameters leading to the modelled efficiencies. It can be observed that positions A and B are associated to similar efficiencies, which is consistent with the type of surrounding materials. Position C, which has fewer interfering objects around the secondary coil, leads to a more efficient performance, even when close to the limit situation in which the coils are not mounted on the vehicle.

If we look closely at these results, we can conclude that the position of the coil (even though it is the same secondary coil)

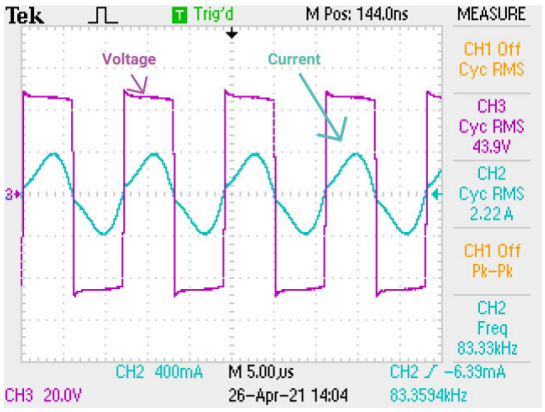

FIGURE 15. Voltage and current at secondary rectifier input (Position C).

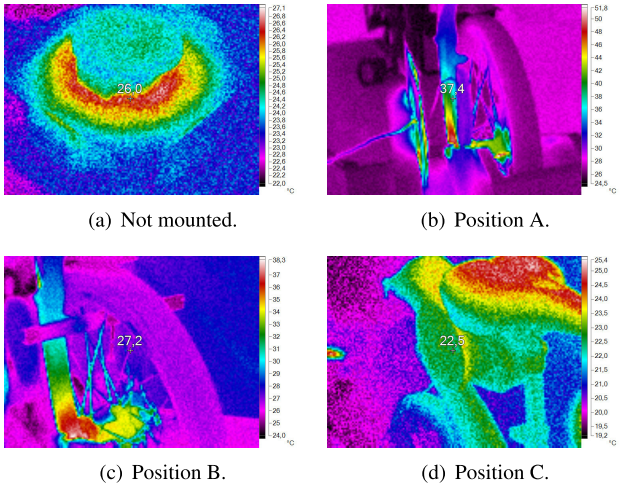

(a) Not mounted. (b) Position A.

(c) Position B. (d) Position C.

FIGURE 16. Temperature measurements in the wireless power transfer for the three tested positions.

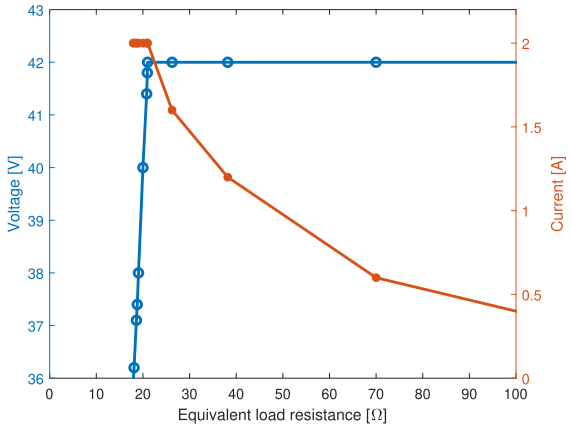

FIGURE 17. Evolution of the charging current and voltage versus battery equivalent resistance in the CV phase.

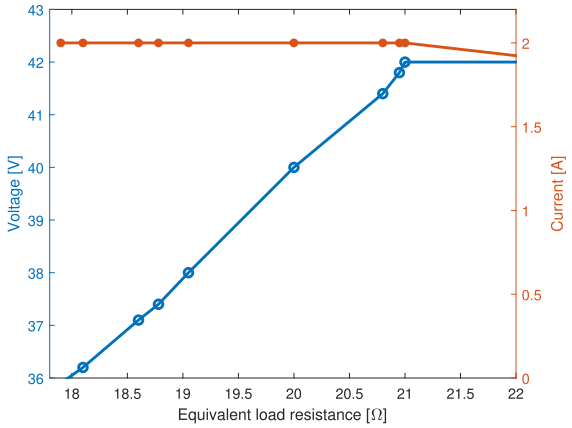

FIGURE 18. Evolution of the charging current and voltage versus battery equivalent resistance in the CC phase.

has a strong impact on the system efficiency for an e-bike charger. In particular, position C is the most efficient, and it approximates the state in which no other conducting material interferes (not mounted). This convenience can be predicted from the measured resistances presented in Table 5. This suitability can also be seen in the heating of the bicycle structure. With a thermal camera, we measured the temperature of the bicycle chassis. The results obtained are shown in Figure 16. As can be observed, position C reaches a lower temperature (approximately 22 °C) in the bicycle material in comparison with the other two positions tested (37.4 °C for position A and 27.2 °C for position B).

Thus, we can conclude that position C is most suitable for our e-bike. For the selected position, we have verified the efficiency of the power converters. From Table 6, we obtained 7.01 W of losses associated to the coupler. For this operation, the inverter and the rectifier losses were 4.32 W and 3.62 W respectively.

In addition, we have checked that the control algorithm implemented in the controller works appropriately. For the specific e-bike model, the battery must be charged at 42 V when a constant-voltage phase is applied and 2 A for a constant-current phase. In Figure 17, the evolution of the charging current and voltage versus the battery equivalent resistance is plotted. The CV phase is shown as the second charging interval and starts with an equivalent resistance value of 21 Ω. The equivalent resistance of a conventional battery varies during the CC-CV charge process with a non-proportional relationship. Thus, the first interval of charge (the CC phase) occurs with low variations on the load resistance. In order to correctly evaluate the CC phase and make a correct graphical representation, it is necessary to establish more measurements for lower battery resistance values and plot them separately. A zoomed image is plotted in Figure 18 for lower values of equivalent resistances and the system working in the CC mode. It can be observed how the CC phase keeps a 2 A constant as the current charge while the voltage increases. Alternatively, the CV phase keeps a voltage constant to 42 V during the charge and the current gradually decreases.

During the charge process, the efficiency of the system varies slightly, as shown in Figure 19. In this figure,

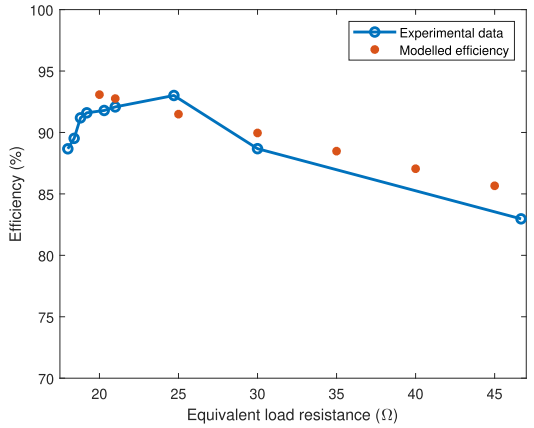

FIGURE 19. Evolution of the efficiency versus battery equivalent resistance.

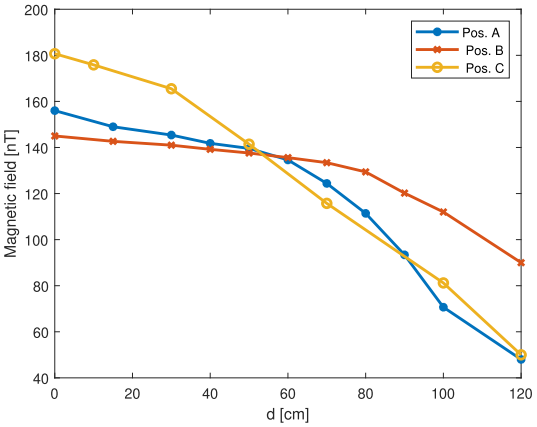

FIGURE 20. Magnetic field measured from the edge of the primary coil.

we have plotted the efficiencies computed from experimental measurements for different load resistances. Please note that the battery resistance increases during the charge in a non-proportional way. We have also included some theoretical efficiencies, which are derived from Equation (10) and the model parameters in Table 5. There is a notable similarity between both data sets.

To complete the performance evaluation of the prototype, we have included the measurement of the magnetic field for the three positions tested. The graph in Figure 20 shows how this parameter evolves with the distance d from the edge of the primary coil.

It can be observed that the field is lower than 27 μT, which is the maximum reference levels for the magnetic flux density for the frequency range between 3 kHz - 10 MHz for general public exposure established by the International Commission on Non-Ionizing Radiation Protection (ICNIRP).

VI. CONCLUSION

E-bikes are foreseen as a convenient mode of transport for future smart cities due to their low cost and easy maintenance. Wireless chargers can encourage the acquisition of these EVs as they bring greater flexibility when charging the battery, which can even be programmable. E-bikes impose strong requirements concerning the weight, costs and size of the components of their wireless charger. These restrictions may be satisfied while achieving a good performance in terms of transfer efficiency and safety. This paper demonstrates the difficulty of resolving two important issues that must be addressed in real e-bikes prototypes. First, we have evaluated the position of the inductive components in the EV wireless charge on the secondary side and how these impact the system efficiency. A theoretical model has been developed and validated with experimental results. Secondly, we propose and evaluate a simple but robust control, particularly suitable for e-bike wireless chargers. With this control, we can conclude that interfering materials impact on the efficiency during the complete charge.

REFERENCES

[1] N. B. Hung and O. Lim, "A review of history, development, design and research of electric bicycles," *Appl. Energy*, vol. 260, Feb. 2020, Art. no. 114323.

[2] R. Citron and J. Gartner, "Executive summary: Electric bicycles Li-ion and SLA E-bikes: Drivetrain, motor, and battery technology trends, competitive landscape, and global market forecasts," Navigant Res., Chicago, IL, USA, Tech. Rep. 1, 2016.

[3] A. Trivino-Cabrera, J. M. Gonzalez-Gonzalez, and J. A. Aguado, *Wireless Power Transfer for Electric Vehicles: Foundations and Design Approach*. Cham, Switzerland: Springer, 2020.

[4] R. Mai, Y. Chen, Y. Li, Y. Zhang, G. Cao, and Z. He, "Inductive power transfer for massive electric bicycles charging based on hybrid topology switching with a single inverter," *IEEE Trans. Power Electron.*, vol. 32, no. 8, pp. 5897–5906, Aug. 2017.

[5] L. A. L. Cardoso, M. C. Marténez, A. A. N. Melendez, and J. L. Afonso, "Dynamic inductive power transfer lane design for E-bikes," in *Proc. IEEE 19th Int. Conf. Intell. Transp. Syst. (ITSC)*. Piscataway, NJ, USA: Institute of Electrical and Electronics Engineers, Nov. 2016, pp. 2307–2312.

[6] S. Liu, X. Li, and L. Yang, "Three-coil structure-based WPT system design for electric bike CC and CV charging without communication," *IET Electr. Power Appl.*, vol. 13, no. 9, pp. 1318–1327, Sep. 2019.

[7] H. Z. Z. Beh, G. A. Covic, and J. T. Boys, "Wireless fleet charging system for electric bicycles," *IEEE J. Emerg. Sel. Topics Power Electron.*, vol. 3, no. 1, pp. 75–86, Mar. 2015.

[8] Y. Chen, N. Yang, B. Yang, R. Dai, Z. He, R. Mai, and S. Gao, "Two-/three-coil hybrid topology and coil design for WPT system charging electric bicycles," *IET Power Electron.*, vol. 12, no. 10, pp. 2501–2512, 2019.

[9] A. Triviño-Cabrera and J. Sánchez, "A review on the fundamentals and practical implementation details of strongly coupled magnetic resonant technology for wireless power transfer," *Energies*, vol. 11, no. 10, p. 2844, Oct. 2018. [Online]. Available: http://www.mdpi.com/1996-1073/11/10/2844

[10] SAE International. (2019). *Wireless Power Transfer for Light-Duty Plug-In/Electric Vehicles and Alignment Methodology (SAE TIR J2954)*. [Online]. Available: https://www.sae.org/standards/content/j2954/

[11] P. K. Joseph, D. Elangovan, and G. Arunkumar, "Linear control of wireless charging for electric bicycles," *Appl. Energy*, vol. 255, Dec. 2019, Art. no. 113898. [Online]. Available: https://www.sciencedirect.com/science/article/pii/S0306261919315855

[12] H. Z. Z. Beh, G. A. Covic, and J. T. Boys, "Investigation of magnetic couplers in bicycle kickstands for wireless charging of electric bicycles," *IEEE J. Emerg. Sel. Topics Power Electron.*, vol. 3, no. 1, pp. 87–100, Mar. 2015.

[13] D. Iannuzzi, L. Rubino, L. P. Di Noia, G. Rubino, and P. Marino, "Resonant inductive power transfer for an E-bike charging station," *Electr. Power Syst. Res.*, vol. 140, pp. 631–642, Nov. 2016.

[14] F. Genco, M. Longo, D. Zaninelli, P. Livrieri, and A. Trivino, "Wireless power transfer system design for E-bikes application," in *Proc. IEEE PES Innov. Smart Grid Technol. Eur. (ISGT-Europe)*. Piscataway, NJ, USA: Institute of Electrical and Electronics Engineers, Oct. 2019, pp. 1–5.

[15] Y. Li, J. Hu, F. Chen, S. Liu, Z. Yan, and Z. He, "A new-variable-coil-structure-based IPT system with load-independent constant output current or voltage for charging electric bicycles," *IEEE Trans. Power Electron.*, vol. 33, no. 10, pp. 8226–8230, Oct. 2018.
[16] Y. Chen, Z. Kou, Y. Zhang, Z. He, R. Mai, and G. Cao, "Hybrid topology with configurable charge current and charge voltage output-based WPT charger for massive electric bicycles," *IEEE J. Emerg. Sel. Topics Power Electron.*, vol. 6, no. 3, pp. 1581–1594, Sep. 2018.
[17] Y. Chen, M. Li, Z. Kou, Z. He, and R. Mai, "Cost-effective inductive power transfer charging system for electric bicycles with variable charging current using primary-side detuned series-series topology," *IET Electr. Power Appl.*, vol. 13, no. 9, pp. 1378–1386, Nov. 2019.
[18] P. K. Joseph, D. Elangovan, and P. Sanjeevikumar, "System architecture, design, and optimization of a flexible wireless charger for renewable energy-powered electric bicycles," *IEEE Syst. J.*, early access, Jun. 1, 2020, doi: 10.1109/JSYST.2020.2993054.
[19] F. Pellitteri, M. Caruso, V. Castiglia, R. Miceli, C. Spataro, and F. Viola, "Experimental investigation on magnetic field effects of IPT for electric bikes," *Electr. Power Compon. Syst.*, vol. 46, no. 2, pp. 125–134, Jan. 2018.
[20] M. Mohammad, E. T. Wodajo, S. Choi, and M. E. Elbuluk, "Modeling and design of passive shield to limit EMF emission and to minimize shield loss in unipolar wireless charging system for EV," *IEEE Trans. Power Electron.*, vol. 34, no. 12, pp. 12235–12245, Dec. 2019.
[21] J. Kim, J. Kim, S. Kong, H. Kim, I.-S. Suh, N. P. Suh, D.-H. Cho, J. Kim, and S. Ahn, "Coil design and shielding methods for a magnetic resonant wireless power transfer system," *Proc. IEEE*, vol. 101, no. 6, pp. 1332–1342, Jun. 2013. [Online]. Available: http://ieeexplore.ieee.org/document/6480778/
[22] Y. Chen, H. Zhang, S.-J. Park, and D.-H. Kim, "A switching hybrid LCC-S compensation topology for constant current/voltage EV wireless charging," *IEEE Access*, vol. 7, pp. 133924–133935, 2019.
[23] H.-N. Vu and W. Choi, "A novel dual full-bridge LLC resonant converter for CC and CV charges of batteries for electric vehicles," *IEEE Trans. Ind. Electron.*, vol. 65, no. 3, pp. 2212–2225, Mar. 2018.
[24] F. Liu, K. Chen, Z. Zhao, K. Li, and L. Yuan, "Transmitter-side control of both the CC and CV modes for the wireless EV charging system with the weak communication," *IEEE J. Emerg. Sel. Topics Power Electron.*, vol. 6, no. 2, pp. 955–965, Jun. 2018.
[25] W. Khan, F. Ahmad, and M. S. Alam, "Fast EV charging station integration with grid ensuring optimal and quality power exchange," *Eng. Sci. Technol., Int. J.*, vol. 22, no. 1, pp. 143–152, Feb. 2019.
[26] D. H. Tran, V. B. Vu, and W. Choi, "Design of a high-efficiency wireless power transfer system with intermediate coils for the on-board chargers of electric vehicles," *IEEE Trans. Power Electron.*, vol. 33, no. 1, pp. 175–187, Jan. 2018.

ALICIA TRIVIÑO-CABRERA was born in Málaga, Spain. She received the master's degrees in telecommunication engineering and computer science engineering from the University of Málaga, Spain, in 2002 and 2008, respectively. Her thesis, which was defended in 2007, focused on wireless networks.

She is currently working as an Associate Professor with the University of Málaga. In the area related to electric vehicles wireless chargers, she has actively participated in the design and development of three prototypes, including features as bi-directionality and dynamic charge. Since 2011, her research interest includes wireless power transfer.

JOSE M. GONZÁLEZ-GONZÁLEZ was born in Málaga, Spain. He received the master's degree in industrial engineering from the University of Málaga, Spain, in 2015. He is currently pursuing the Ph.D. degree in wireless power transfer in electric vehicles, focused on the design of a prototype with bidirectional features. He also has practical experience working on smart grids and renewable energy projects, with some publications on the integration of battery energy storage.

JOSÉ A. AGUADO (Member, IEEE) was born in Málaga, Spain. He received the degree in electrical engineering and the Ph.D. degree from the University of Málaga, Málaga, in 1997 and 2001, respectively.

He is currently a Full Professor and the Head of the Electrical Engineering Department, University of Málaga, Spain. He has led more than 40 publicly funded research and consulting projects on the operation and planning of smart grids and wireless power transfer.